Contributed paper

OPTO-ELECTRONICS REVIEW **9**(4), 423–430 (2001)

A device for light scatterometry on single levitated droplets

D. JAKUBCZYK, M. ZIENTARA, W. BAZHAN, M. KOLWAS* and K. KOLWAS

Institute of Physics of the Polish Academy of Sciences,
32/46 Lotników Ave., 02-668 Warsaw, Poland

A compact device for measurements of levitated particles in humid atmosphere up to 100% relative humidity and in temperature range from –30 to 60°C was built. The preliminary experiments were done using ethanediol and water microdroplets. Light scattered by the trapped particles on two perpendicular polarisations was recorded. On the basis of Mie theory information on the radius and refractive index of the droplets was extracted with FFT and T-matrix method combined with fitting procedure.

Keywords: light scattering, electrodynamic trap, microparticles levitation, water microdroplets, climatic microchamber.

1. Introduction

Meteorological models and climate simulations require incorporating microphysics of clouds and aerosols for their proper operation [1,2]. Sound knowledge of the properties of clouds and aerosols at microscopic level would also yield a better interpretation of remote sensing of atmosphere (e.g. lidar, Ref. 3). Fortunately microphysics may be explored experimentally. There is a vast number of experimental works in this field, though the need for more is not diminishing. There is quite a number of well established experimental techniques of investigation of individual microparticles, such as localised calorimetric analysis [4], shock-tube methods [5], Knudsen cells [6] or monodisperse droplet streams [7,8], but relatively recent techniques of levitation seem to prevail. There are ultrasonic [9,10], optical [11] and electrodynamic levitators [12,13]. In this work we concentrate on electrodynamic levitation of water droplets as suitable for objects of sizes between 0.1 and 250 μm.

It appeared to us that some of the experimental work pertaining to the microphenomena concerning water in the earth atmosphere has been done under quite unrealistic conditions, such as very low pressures, low relative humidity or in inert atmospheres (compare e.g., Ref. 14). We understand that this was the way around such problems like electrical discharges, effects of free convection or photophoretic forces. Thought the results of such experiments are possibly quite valid, we tried a straightforward way and levitated water droplets in realistic humid atmosphere. We also aimed at tropospheric conditions rather than the stratospheric ones (compare e.g., Ref. 15).

*e-mail: kolwas@ifpan.edu.pl

2. Experimental setup

2.1. Trap

The electromagnetic Paul type trap presented in Fig. 1 constitutes the heart of the apparatus. The electrodes of the trap are close to but not strictly hyperboloidal (they are prepared by pressing). Their precise shape is not crucial for the particles that we encounter (micrometers' size liquid droplets). The caps are painted with insulating enamel to suppress electric discharges due to the humid environment and the ring is painted with graphite in order to both reduce stray light scattering and suppress uneven charge accumulation (from charged droplets falling on the ring) which in turn prevents trapping field distortion. The trap holder is made of polysilane and is equipped with air-tight through-leads for trap driving voltage and a port for a thermocouple. The AC driving voltage applied between the caps and the ring is supplied via resistors by a HV 1:66 transformer fed from the amplifier fed in turn from Keithley function generator set to sine wave. Usually we use ~3000 V RMS at ~290 Hz. Apart from that we can apply a DC voltage (usually several volts) between the caps and thus control the position of the trapped droplet along the vertical axis. The essential technical detail is that every electrode is driven via resistor. The total resistance in drive path is 100 MΩ and this is the main factor inhibiting discharges and thus enabling us to operate in humid atmosphere.

2.2. Droplet injector

Our droplet injector is a bubble-jet type device (compare e.g., Ref. 16). We present it in Fig. 2. We discharge a 10 μF capacitor charged to ~250 V through a ~7 mm resistive (kantal) wire – heater immersed in the liquid thus producing a pressure wave which ejects a single or few droplets

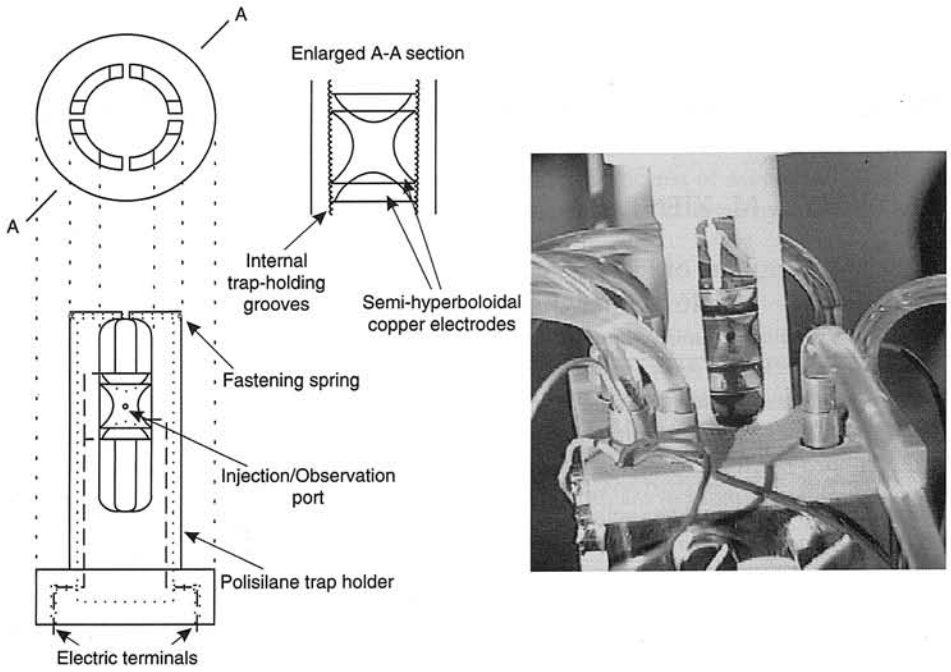

Fig. 1. Electrodynamic trap in the holder.

through a special nozzle. We make nozzles of desired diameter by pulling, cutting and polishing of glass tube. It has been found that the wall thickness around the very nozzle should be considerable (several diameters of the opening) and the cone angle of the channel preceding the nozzle should be nearly right. The liquid is contained in a thick-walled tubular cuvette closed at one end with exchangeable nozzle and through the other end the power leads of the heater are introduced. There is a 3rd port in the middle pointing upwards through which the liquid is poured in. Droplets are injected through a 3-mm diameter port in the ring electrode. The injection timing is precisely controlled with a digital delay circuit utilising the trap driving AC signal as the reference.

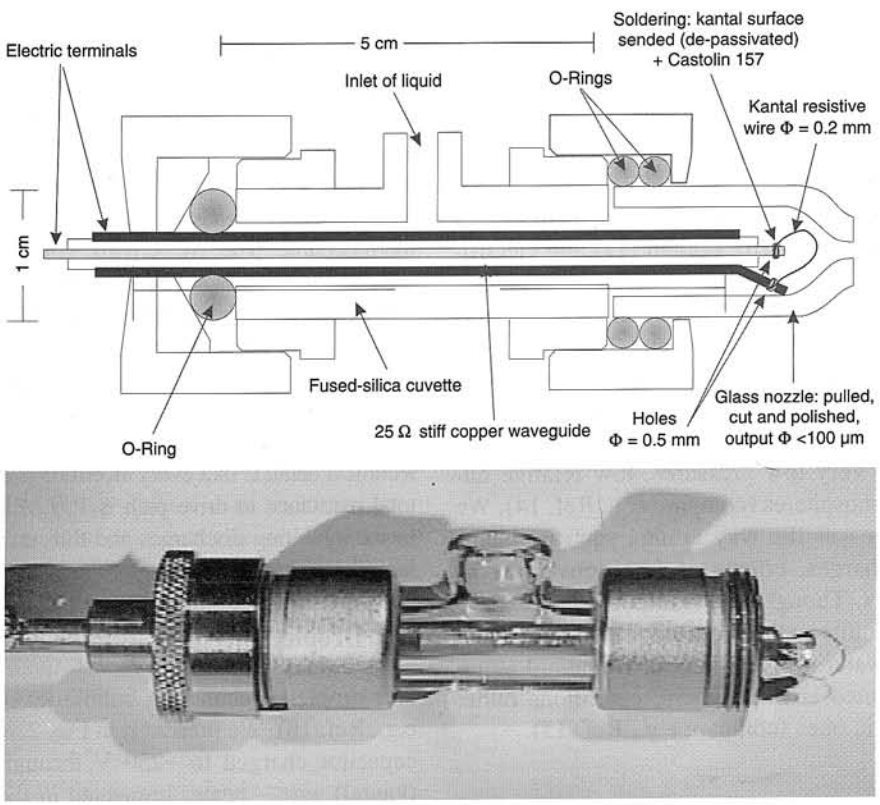

Fig. 2. Droplet injector.

2.3. Climatic microchamber

The trap holder from the top and the droplet injector from the side are inserted into the ports of a double-walled air tight chamber – presented in Fig. 3 – which can be cooled/heated with Peltier elements. Each Peltier element is in turn cooled with water. The cooling mechanism is quite efficient so that we can go below dew point in about 30 s and down to –30°C in several minutes. Temperature inside the cell is measured with a T-type thermocouple.

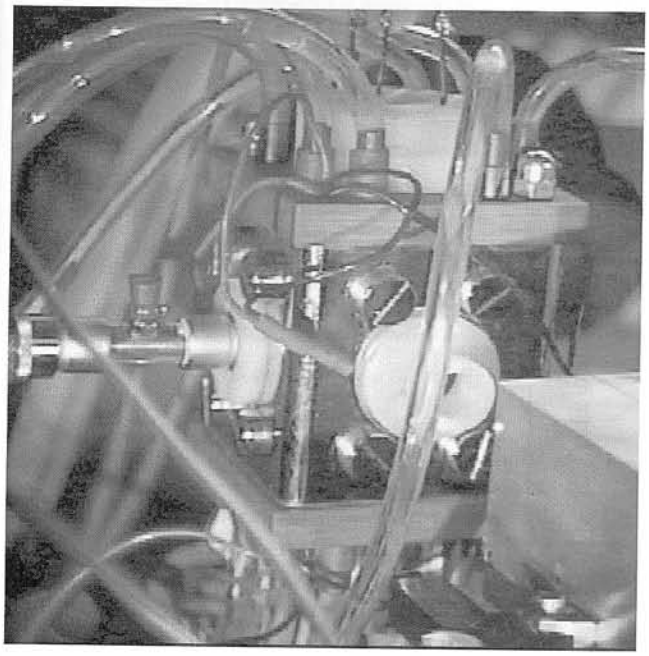

Fig. 3. Climatic microchamber.

The bottom port can be used to control the pressure and the composition of the atmosphere inside the chamber. Thus we should be able to simulate the conditions and the dynamics of the upper troposphere. On the other hand heating and evacuating the chamber should enable us to get rid of unwanted liquid deposits (lost droplets) without taking out the trap.

2.4. Optical system

The chamber port and the 3-mm diameter port in the trap ring opposite to the droplet injector are used for introducing the laser beam (He-Ne 632 nm, 7 mW CW) into the trap (see Figs. 3 and 4). It propagates precisely upstream the injected particles and illuminates trapped particles. The laser head is tilted so that the polarisation is 45° off vertical. This enables us to observe the scattered light at both *p* and *s* polarisation geometries. As a matter of fact it also enables us to observe crossed polarisations *ps* and *sp* which can arise from nonsphericity of the droplet and thus measure such. The scattered light is collected at right angle through another 3-mm diameter port in the ring electrode with a microscope objective (Fig. 4) inserted into a chamber side port perpendicular to the injector and laser beam. The objective is characterised with a relatively large numerical aperture (DIN 10×, NA = 0.3) though we do not use it along the DIN standard. The objective has been reassembled into a plastic body in order to suppress electrical and reduce thermal conductivity. The metal holder of the entrance lens which could not be removed has been equipped with a spring to provide electrical contact with the trap ring. This objective enables us to collect light from a cone of about 17°. Behind the objective, just in front of

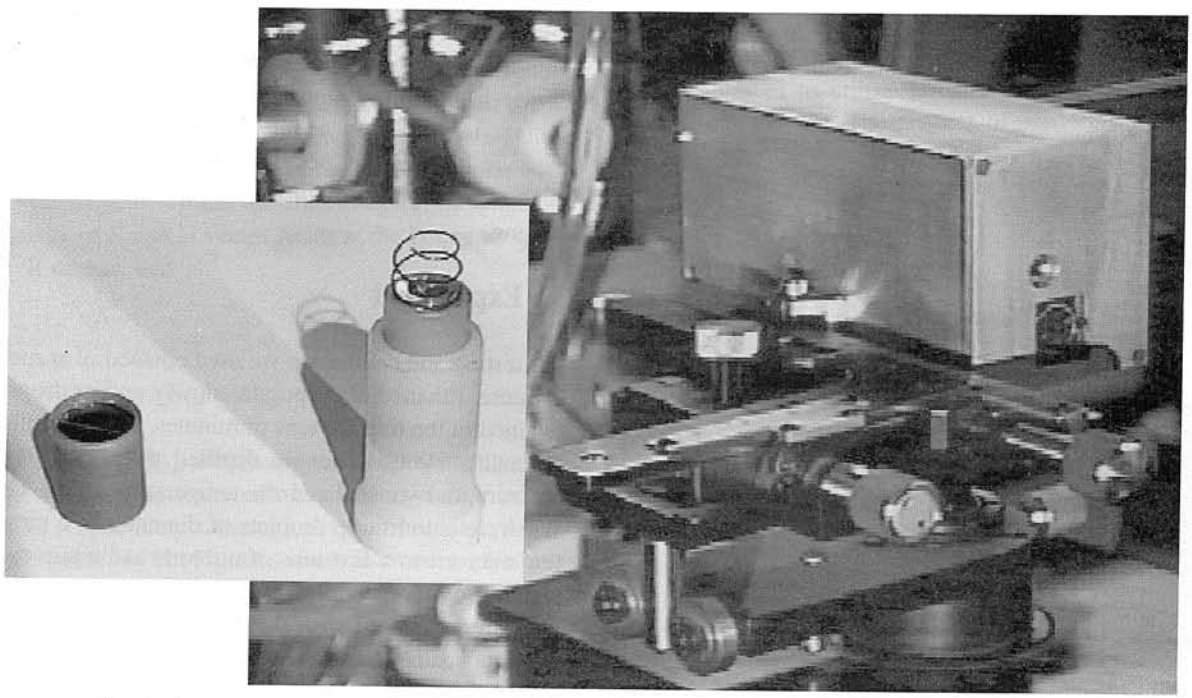

Fig. 4. CCD camera on the micromanipulator. Objective (compare main picture) and polariser (inset).

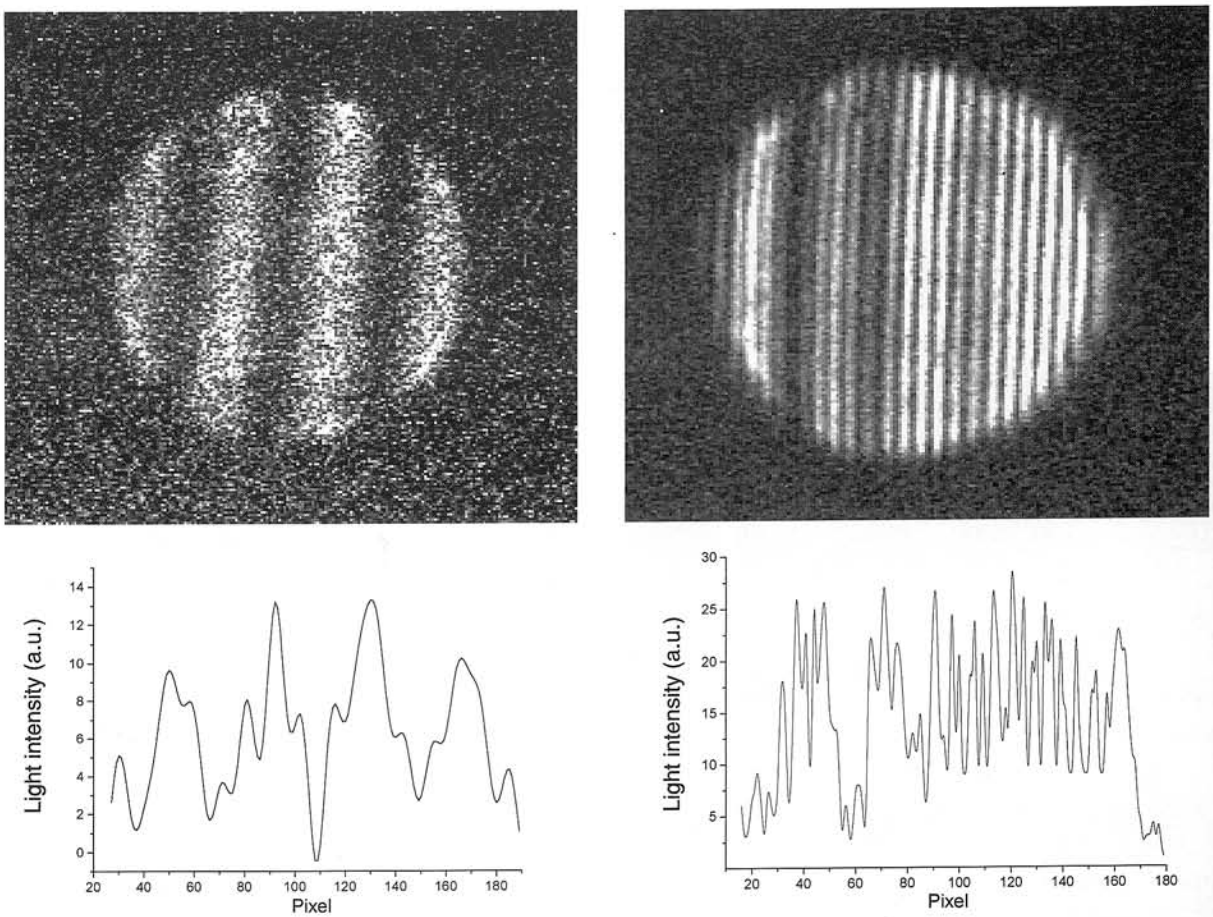

Fig. 5. Scatterogram of ethanediol droplets of ~2 μm (left) and ~20-μm radii (right); below: intensity profiles at the equator. Left intensity profile has been smoothed.

the CCD there are two semicircular sheet polarisers with polarisation directions set perpendicularly dividing the field of view into two semicircles. This enables us to record scattering images on both polarisations simultaneously (compare Fig. 6). The images are collected with a B/W CCD camera (Fig. 4) with gain control usually set to manual. The objective-camera system is set so that the object plane lies in front or behind the actual object (droplet). In this way we observe Mie interference patterns convoluted with the aperture rather than the surface of the droplet. Otherwise it would be impossible to resolve the fringes. The camera is placed on a micromanipulator so that we can measure its (relative) position with 0.1-mm precision. The images are digitised with a frame-grabber for further processing.

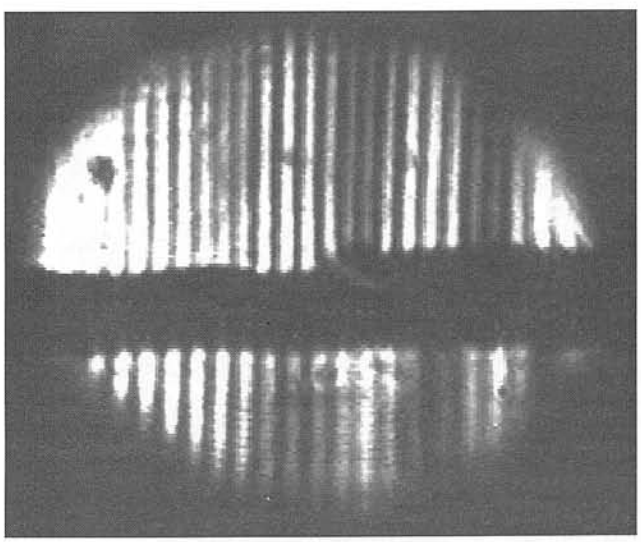

Fig. 6. Scatterogram of a ~20 μm's radius droplet taken on *p* and *s* polarisation simultaneously.

3. Experiment

For testing and calibration we used ethanediol at room temperature. Ethanediol evaporates slowly and its drops can be retained in the trap for tens of minutes. For preliminary experiments we used doubly distilled water at atmospheric pressure and we lowered the temperature in the chamber. We were able to trap droplets of diameter in a range from few microns to a few tens of microns and retain them, depending on temperature, for a few seconds to a few minutes. In agreement with the Mie theory prediction, small droplets scatter significantly less light than large droplets and thus scatterograms of small droplets present much lower S/N ratio. However, scatterograms of larger droplets

present a denser pattern of fringes which at the set magnification causes resolution problems. In view of that we intend to both improve digitisation accuracy and to use of a more powerful laser and possibly shorter wavelength. We were also able to trap a few droplets simultaneously. An example of that is presented in Fig. 7: a droplet in the very centre of the trap is surrounded by 3 others all laying in the equatorial plane of the trap. These satellite droplets undergo stronger macromotion and are lost more easily.

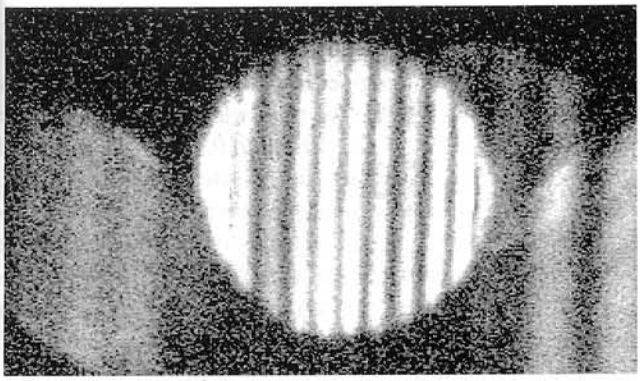

Fig. 7. Four droplets in the trap.

3.1. Scattering of light – Mie theory

When a polarised plane harmonic E-M wave falls on a microdrop of water, it is scattered. This results in a propagation of a scattered E-M wave around the microdrop. This new wave can be described as a superposition of an infinite number of elementary waves. The amplitude of this wave takes the form of a constant E-M multifield. Thus an interference imagine of the microdrop may form. The problem of the scattering of a polarised plane E-M wave on a sphere was solved by Gustav Mie in 1908 [17,18]. He gave mathematical formulas, that describe the electric $\mathbf{E}_s$ and magnetic $\mathbf{H}_s$ vector fields of scattered wave. He assumed that the incident wave ($\mathbf{E}_i = E_0 e^{ikr\cos\theta}\mathbf{e}_z$, $\mathbf{H}_i$) was falling on a spherical particle resting at the origin of the spherical polar coordinate system (r, ϕ, θ) and the continuity of the tangential components of $\mathbf{E}$ and $\mathbf{H}$ vector fields at the boundary of the sphere. It means, that

$$E_{i\theta} + E_{s\theta} = E_{I\theta} \tag{1}$$

$$E_{i\phi} + E_{s\phi} = E_{I\phi} \tag{2}$$

where $\mathbf{E}_{i\theta,\phi}$, $\mathbf{E}_{s\theta,\phi}$, $\mathbf{E}_{I\theta,\phi}$ are the tangential components of the incident wave $\mathbf{E}_i$, the scattered wave $\mathbf{E}_s$ and wave inside the sphere $\mathbf{E}_I$ respectively. Analogical equations describe the magnetic fields $\mathbf{H}_i$, $\mathbf{H}_s$, $\mathbf{H}_I$. As a result he obtained formulas for the scattered wave

$$\vec{E}_s = \sum_{n=1}^{\infty} E_n (i a_n \vec{N}_{e\ln}^{(3)} - b_n \vec{M}_{e\ln}^{(3)}) \tag{3}$$

$$\vec{H}_s = \sum_{n=1}^{\infty} E_n (i b_n \vec{N}_{o\ln}^{(3)} - a_n \vec{M}_{e\ln}^{(3)}) \tag{4}$$

$$E_n = i^n E_0 \frac{2n+1}{n(n+1)} \tag{5}$$

The functions $\boldsymbol{N}_{e\ln}^{(3)}$, $\boldsymbol{M}_{o\ln}^{(3)}$ and $\boldsymbol{N}_{o\ln}^{(3)}$, $\boldsymbol{M}_{e\ln}^{(3)}$ are involved sums of products of $\sin(\phi)$ or $\cos(\phi)$ functions, the associated Legendre polynomials of the first kind of the first order $P_n^1[\cos(\theta)]$ and the Basel functions of the third kind (the Henkel functions) $h(kr)$ (k is a wave number). The coefficients a_n and b_n take the form of

$$a_n = \frac{m\psi_n(mx)\psi_n'(x) - \psi_n(x)\psi_n'(mx)}{m\psi_n(mx)\xi_n'(x) - \xi_n(x)\psi_n'(mx)} \tag{6}$$

$$b_n = \frac{\psi_n(mx)\psi_n'(x) - m\psi_n(x)\psi_n'(mx)}{\psi_n(mx)\xi_n'(x) - m\xi_n(x)\psi_n'(mx)} \tag{7}$$

where ψ_n and ξ_n are the Riccati-Basel functions depending on relative refractive index m and size parameter x defined as follows

$$x = ka = \frac{2\pi n_2 a}{\lambda} \tag{8}$$

$$m = \frac{n_1}{n} \tag{9}$$

where a and n_2 are the radius and the refractive index of a microdrop respectively, n_1 is the refractive index of a medium surrounding the microdrop and λ is the wavelength of the incident wave.

Such form of the mathematical formulas describing the field enables us to utilise T-matrix method for numerical calculations [19,20]. The process of scattering is than described as

$$\begin{pmatrix} E_s^p \\ E_s^s \end{pmatrix} = \frac{\exp(ikr - z)}{-ikr} \begin{pmatrix} S_1 & 0 \\ 0 & S_2 \end{pmatrix} \begin{pmatrix} E_i^p \\ E_i^s \end{pmatrix} \tag{10}$$

where superscripts denote polarisation and z is the distance in the direction of the incident wave. It is worth stressing that the amplitude matrix $\mathbf{S}$ carries information about the properties of scattering particle only. The elements S_1 and S_2 are functions of ϕ, θ and may be expressed in terms of the coefficients a_n and b_n as follows

$$S_1 = \sum_n \frac{2n}{n(n+1)} (a_n \pi_n + b_n \tau_n) \tag{11}$$

$$S_2 = \sum_n \frac{2n}{n(n+1)}(a_n\tau_n + b_n\pi_n) \tag{12}$$

where $\pi_n = P_n^1/\sin\theta$ and $\tau_n = dP_n^1/d\theta$. Since it is only the intensity of the scattered light that is accessible with measurement, a scalar description of the process is adequate. Fortunately, the intensity of scattered light on both polarisations can be expressed by means of **S** matrix elements as follows

$$\begin{aligned} i_p &= S_{11} + S_{12} \\ i_s &= S_{11} - S_{12} \end{aligned} \tag{13}$$

where

$$\begin{aligned} S_{11} &= \frac{1}{2}\left(|S_2|^2 + |S_1|^2\right) \\ S_{12} &= \frac{1}{2}\left(|S_2|^2 - |S_1|^2\right) \end{aligned} \tag{14}$$

If we also define

$$\begin{aligned} S_{33} &= \frac{1}{2}(S_2^* S_1 + S_2 S_1^*) \\ S_{34} &= \frac{i}{2}(S_2^* S_1 - S_2 S_1^*) \end{aligned} \tag{15}$$

Stocks' parameters of a monochromatic transverse wave can be conveniently calculated with T-matrix method

$$\begin{pmatrix} I_s \\ Q_s \\ U_s \\ V_s \end{pmatrix} = \frac{1}{k^2 r^2} \begin{pmatrix} S_{11} & S_{12} & 0 & 0 \\ S_{12} & S_{11} & 0 & 0 \\ 0 & 0 & S_{33} & S_{34} \\ 0 & 0 & -S_{34} & S_{33} \end{pmatrix} \tag{16}$$

thus yielding a complete scalar description of the field.

3.2. Processing of experimental data

The scatterogram (interference image) recorded during the experiment presents the scattered light intensity I as a function of angles θ (azimuth when in the observation plane) and ϕ (elevation). However, the scatterogram is recorded in the form of a bitmap and requires pixel to angle calibration to suit analytical Mie formulas. This calibration requires conceptually elementary measurements of geometrical relations of the imaging system or utilising of a calibration sphere of perfectly known size and refractive index. The first seemed better (and easier) to us. However, the mechanical construction of our imaging system enabled only the precision of calibration of about 3%. We intend to improve the construction, but so far the amendment is achieved with software (see below). Calibrated scatterogram can be fitted with Mie formula and relevant information can be extracted.

The fitting procedure is based on the matrix formulation of Mie theory. In every iteration a theoretical interference pattern for a given range of θ and the $\phi = \pi/2$ (the dependence on ϕ within ±17° off scattering plane is relatively weak and can be neglected) is calculated. There are seven parameters available in the procedure. These are: the incident field wavelength λ, the radius R and the refractive index n_2 of the particle, the refractive index of the surrounding medium n_1, the intensity scaling factor P_0 (the measured intensity is not and can not easily be calibrated) and two parameters P_1 and P_2 enabling refining of pixel to angle calibration: $(P_1 + P_2\,\phi)$. According to our experimental conditions we fix λ = 632.8 nm and n_1 = 1. Assuming perfect calibration, we initially fix P_1 = 0 and P_2 = 1. Since we used water, we initiated n_2 = 1.3328 (value for 632.8 nm, 10°C and 0.1 Mpa, Ref. 21) and eventually allowed varying at the later stages of fitting. Since there is a linear dependence between R and the predominant space (or angle) frequency of FFT of $I(\theta)$ for the vertical polarisation of the scattered waves [22], the parameter R could be initiated that way. It is worth noting that for many applications an approximate value of R given by FFT (±5%) is sufficient.

The calculations were being carried alternately for horizontal and vertical polarisations, until the results obtained for them were similar. The difference between them was smaller then the minimal estimated error of any of them which is 3% (calibration limit).

3.3. Size and refractive index of a droplet

Below we present results for two ambient temperatures T_a: 5°C and –28°C. In both cases the temperature of injected droplet T_d = 5°C and the 100% relative humidity (RH) was ensured by the wet cotton-wool at the bottom of the chamber. Five and six unambiguous frames could be chosen from the recorded avi file respectively. The example of obtained scatterogram profiles together with appropriate fits are presented in Figs. 8 and 9. On the basis of the contrast of the scatterogram we judge that all presented data points correspond to a liquid droplet (compare e.g. Ref. 23). In case of T_a = –28°C, some or all presented points may correspond to a supercooled liquid, since the droplet heat was

Table 1. The evolution of R and n of the droplet for T_a = 5°C.

	R (μm)		n	
t (s)	I_s	I_p	I_s	I_p
2.58	7.1	7.1	1.3328	1.3328
2.83	6.8	6.8	1.3328	1.3328
3.33	5.8	5.8	1.3328	1.3328
5.33	4.3	4.3	1.3328	1.3328
6.25	3.9	3.9	1.3328	1.3328
15	3.01	2.99	1.3328	1.3328

being lost due to conduction, radiation and evaporation for a few seconds prior to the presented sequence. The behaviour of R and n of the droplets in time was studied and is collected in Tables 1 and 2 and in Fig. 10.

Table 2. The evolution of R and n of the droplet for $T_a = -28$°C.

	R (μm)		n	
t (s)	I_s	I_p	I_s	I_p
1.75	8.5	8.6	1.3328	1.3328
2.08	6.6	6.6	1.3328	1.3328
2.33	6.1	6.2	1.3328	1.3328
2.83	–	5.1	1.3328	1.3328
3.25	4.2	4.2	1.3328	1.3328

where t is time (start time was arbitrary in both cases), I_s and I_p are scattered light intensities on s and p polarisation, respectively.

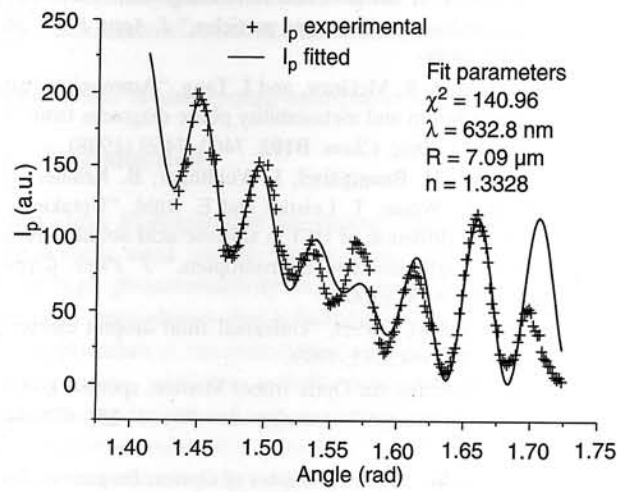

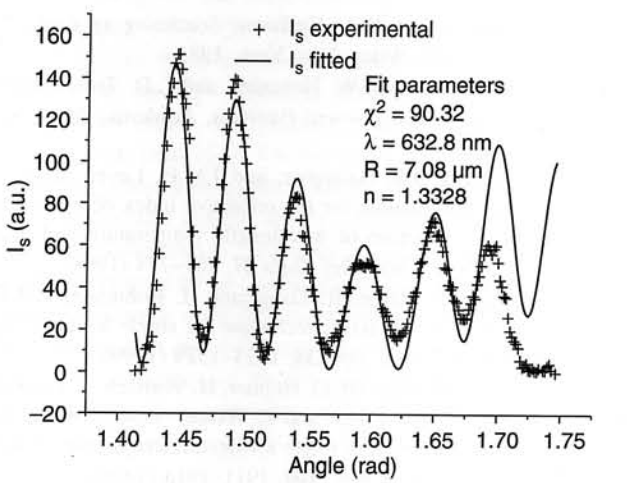

Fig. 8. The averaged sections of the scatterograms and Mie theory fits for the droplet at 5°C ambient temperature.

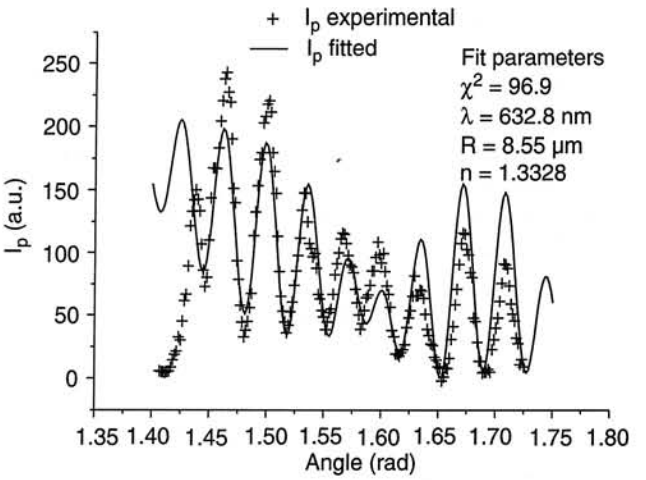

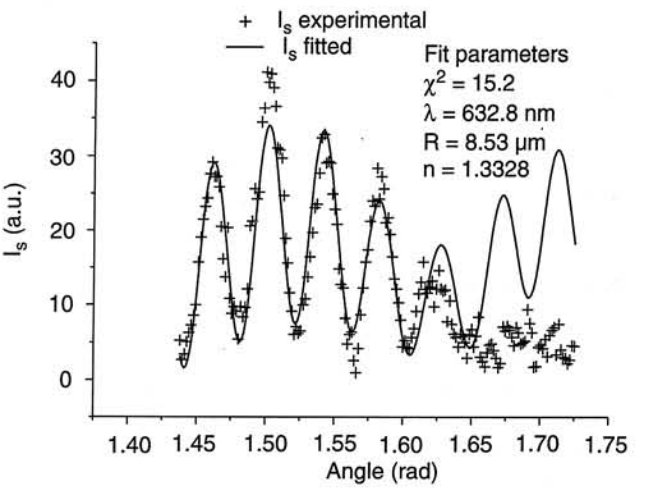

Fig. 9. The averaged sections of the scatterograms and Mie theory fits for the droplet at –28°C ambient temperature.

The refractive index turned out to be the same for all the cases, which was rather intuitive, but for both temperatures T_a slightly off the expected value. Allowing no constraints eventually produced nonphysical values. Manual adjustments deteriorated χ^2 *of the fit.*

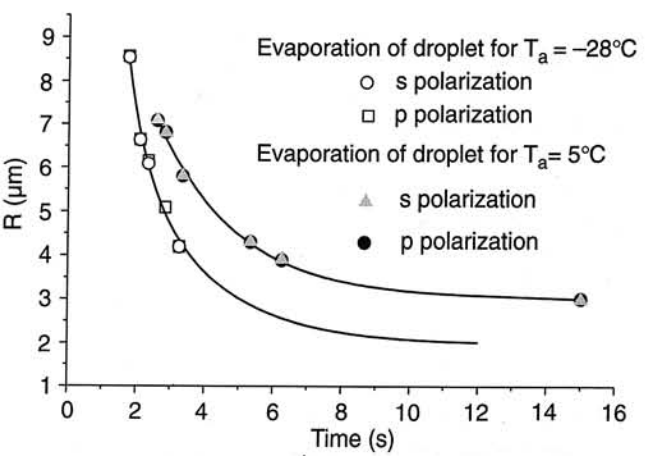

Fig. 10. Evaporation of two droplets at 5°C and at –28°C ambient temperature.

Calculations show that the pressure added to the interior of the droplet by the surface tension (R dependent) is in our cases always below 10^5 Pa (it is also countered by the presence of surface charge) and has negligible (10^{-6}) influence upon n. Thus the stabilisation of n seems to be a software effect. However, in order to tackle the problem we first have to improve the quality of our scatterograms, since they may be considerably distorted at the brims. The possible sources of deformations are effects of the apertures of the observing system (vignetting) and eventually the properties of the lenses. All these may change the relations between maxima and minima of the scatterogram and mislead the fitting procedure. The smaller the droplet, the fewer interference fringes, the higher impact of deformations and the lower precision.

The radius R seemed to be easier to handle though for the reasons given above the precision of the results is not overwhelmingly better than that of the already mentioned FFT method.

Our present experience allows us to state that the space frequency of appearance of the interference fringes depends stronger on R then on n, however, the amplitude of fringes is stronger influenced by n.

4. Conclusions

A device suitable for measurements of levitated particles in realistic tropospheric conditions was built and found operational. It features modular flexible construction enabling easy modifications for wide range of applications. Paul type quadrupole electrodynamic trap constitutes the heart of the apparatus. The preliminary calibration and measurements were performed using ethanediol and water microdroplets. Scattering of light was used as a measuring tool. Scatterograms were processed with the aid of Mie theory formalism. FFT and T-matrix methods were utilised as numerical tools for extracting the radius and the refractive index of the droplets.

References

1. S.E. Schwart, F. Arnold, J.P. Blanchet, P.A. Durkee, D.J. Hofmann, W.A. Hoppel, M.D. King, A.A. Lacis, T. Nakajima, J.A. Ogren, O.B. Toon, and M. Wendisch, "Group report: Connections between aerosol properties and forcing of climate,"' in *Aerosol Forcing of Climate*, pp. 251–280, edited by Charlson and Heintzenberg, Wiley, New York, 1995.
2. H.R. Pruppacher and J.D. Klett, *Microphysics of Clouds and Precipitation*, Kluwer, Dordrecht, 1998.
3. D.R. Cutten, J.D. Spinhirne, R.T. Menzies, D.A. Bowdle, V. Srivastava, R.F. Peuschel, A.D. Clarke, and J. Rothermal, "'Intercomparisons of pulsed lidar data with flight level CW lidar data and modelled backscatter from measured aerosol microphysics near Japan and Hawaii," *J. Geophys. Res.* **103**, 19649–19661 (1998).
4. H.M. Pollock and A. Hammiche, "'Micro-thermal analysis: techniques and applications," *J Phys. D: Appl Phys* **34**, R23–R53 (2001).
5. R.A. Zahoransky, J. Hoschele, and J. Steinwandel, "Formation of argon clusters by homogeneous nucleation in supersonic shock tube flow," *J. Chem. Phys.* **103**, 9038–9044 (1995).
6. A.L. Goodman, G.M. Underwood, and V.H. Grassian, "A laboratory study of the heterogeneous reaction of nitric acid on calcium carbonate particles," *J. Geophys. Res.* **105**, 29053–29064 (2000).
7. R.N. Berglund and B.Y.H. Liu, *Environ. Sci. Technol.* **7**, 147 (1973).
8. K.H. Fung and I.N. Tang, "Chemical characterisation of aerosol particles by laser Raman spectroscopy," in *Aerosol Chemical Processes in the Environment*, pp. 177–195, edited by K.R. Spurny and D. Hochrainer, CRC Press LLC, Boca Raton, 2000.
9. E.G. Lierke, "Acoustic levitation – a comprehensive survey of principles and applications," *Acoustica* **82**, 220–237 (1996).
10. S. Bauerecker and B. Neidhart, "Cold gas traps for ice particle formation," *Science* **282**, 2211–2212 (1998).
11. A. Ashkin, "'Optical trapping and manipulation of neutral particles using lasers," *Proc. Natl. Acad. Sci. USA* **94**, 4853–4860 (1997).
12. W. Paul, "Electromagnetic traps for charged and neutral particles," *Rev. Mod. Phys.* **62**, 531–540 (1990).
13. R.F. Wuerker, H. Shelton, and R.V. Langmuir, "Electrodynamic containment of charged particles," *J. Appl. Phys.* **30**, 342–349 (1959).
14. J. Xu, D. Imre, R. McGraw, and I. Tang, "Ammonium sulfate: Equilibrium and metastability phase diagrams from 40 to –50°C," *J. Phys. Chem.* **B102**, 7462–7469 (1998).
15. M. Schwell, H. Baumgärtel, I. Weidinger, B. Krämer, H. Vortisch, L. Wöste, T. Leisner and E. Rühl, "Uptake dynamics and diffusion of HCl in sulfuric acid solution measured in single levitated microdroplets," *J. Phys. Chem.* **A104**, 6726–6732 (2000).
16. E.R. Lee and M.L. Perl, "Universal fluid droplet ejector," U.S. Pat. No. 5943075, 1999.
17. G. Mie, "Beiträge zur Optik trüber Medien, speziell kolloidaler Metallösungen," *Annalen der Physik* **25**, 377–445 (1908).
18. M. Born and E. Wolf, *Principles of Optics*, Pergamon, Oxford, 1970.
19. C.F. Bohren and D.R. Huffman, *Scattering of Light by Small Particles*, Wiley, New York, 1983.
20. M.I. Mishschenko, J.W. Hovenier, and L.D. Travis, *Light Scattering by Nonspherical Particles*, Academic Press, San Diego, 2000.
21. A.H. Harvey, J.S. Gallagher, and J.M.H. Levelt Sengers, "Revised formulation for the refractive index of water and steam as a function of wavelength, temperature and density," *J. Phys. Chem. Ref. Data* **27**, 761–774 (1998).
22. B. Steiner, B. Berge, R. Gausmann, J. Rohmann, and E. Rühl, "Fast in situ sizing technique for single levitated liquid aerosols," *Appl. Opt.* **38**, 1523–1529 (1999).
23. B. Krämer, M. Schwell, O. Hübner, H. Vortisch, T. Leisner, E. Rühl, H. Baumgärtel, and L. Wöste, "Homogeneous ice nucleation observed in single levitated micro droplets," *Ber. Bunsenges. Phys. Chem.* **100**, 1911–1914 (1996).

